Available online at www.sciencedirect.com

SciVerse ScienceDirect

Ceramics International 38 (2012) 6677–6684

CERAMICS INTERNATIONAL

www.elsevier.com/locate/ceramint

Effect of MgO addition on the crystallization and in vitro bioactivity of glass ceramics in the $CaO–MgO–SiO_2–P_2O_5$ system

J. Ma[a,b,c], C.Z. Chen[a,*], D.G. Wang[a], X. Shao[b,c], C.Z. Wang[b,c], H.M. Zhang[d]

[a]*Key Laboratory for Liquid-Solid Structural Evolution and Processing of Materials, Ministry of Education, Shandong University, Shandong Ji'nan 250061, PR China*

[b]*Liaocheng Research Institute of Non-ferrous Metals, Liaocheng University, Shandong Liaocheng 252029, PR China*

[c]*School of Materials Science and Engineering, Liaocheng University, Shandong Liaocheng 252029, PR China*

[d]*Stomatology Department, Liaocheng Hospitial, Shandong Liaocheng 252000, PR China*

Received 14 March 2012; received in revised form 13 May 2012; accepted 18 May 2012
Available online 23 May 2012

Abstract

$CaO–MgO–SiO_2–P_2O_5$ glass ceramics were successfully prepared by sintering the sol–gel-derived powders. The effects of MgO addition on the samples crystallization and structure were investigated by means of differential thermal analysis (DTA), X-ray diffraction (XRD) and scanning electron microscopy (SEM). In addition, samples degradation and in vitro bioactivity assays were also evaluated. With more MgO addition, the glass ceramics crystallization kinetics under non-isothermal conditions changed from bulk crystallization to surface crystallization, and new crystal phases of $Ca_2MgSi_2O_7$ and SiO_2 were induced. In addition, it is observed that with increasing MgO concentration, the glass ceramics degradability gradually decreased and the formation of apatite was delayed.

Keywords: A. Sintering; D. Glass ceramics; D. MgO; E. Biomedical applications

1. Introduction

Many kinds of bioactive inorganic-materials including bioactive glasses, glass ceramics and calcium phosphate ceramics have been developed during the past few decades, and some of them are applied to repair and reconstruct diseased or damaged bones or tissues [1–4]. In the last years, bioactive glass ceramics attract particular interest for possible clinic applications, because these glass ceramics provide great possibilities to manipulate their properties, such as transparency, strength, resistance to abrasion, coefficient of thermal expansion and bioactivity [5–7]. In essence, these variations in properties depend on samples composition, which have great effect on the extent of crystallization, crystal phase, morphology and size. Meanwhile, modification of the crystallization paths and kinetics is also interesting since it can be exploited to tailor a great range of samples properties and to favor their application.

Magnesium, one important trace element, can be observed in human body and critical concentration shows a principal function on constituting of human bones and teeth, such as enamel, dentin and bone contain 0.44, 1.23 and 0.72 wt% of magnesium, respectively. It has been reported that magnesium plays an important role in human bone development, maintenance and repair through stimulating osteoblast proliferation [8–10]. In addition, critical content of magnesium can modulate the glass dissolution or physico-chemical reactions occurring at the material periphery [11–13].

In view of the effect of the magnesium and crystallization on the samples structure and properties, this paper indicates the studies of the crystallization behavior of $CaO–SiO_2–P_2O_5$ system and its derivative of $CaO–MgO–SiO_2–P_2O_5$, where CaO was gradually substituted by MgO with the same mole percent. In

*Corresponding author. Tel.: +86 531 88395991; fax: +86 531 88395991.
E-mail address: czchen@sdu.edu.cn (C.Z. Chen).

0272-8842/$36.00
http://dx.doi.org/10.1016/j.ceramint.2012.05.056

addition, the samples structure and in vitro bioactivity are also investigated.

2. Experimental procedure

2.1. Materials and sample preparation

Four samples, with compositions presented in the Table 1, were synthesized by the sol–gel technique. Briefly, glass synthesis was carried out by hydrolysis and polycondensation of appropriate amounts of tetraethyl orthosilicate (TEOS), triethyl phosphate (TEP), calcium nitrate ($Ca(NO_3)_2 \cdot 4H_2O$) and magnesium nitrate ($Mg(NO_3)_2 \cdot 6H_2O$) in deionized water with a molar ratio of H_2O/(TEOS+TEP)=10. Nitric acid (HNO_3, 2N) was added to catalyze the hydrolysis of TEOS and TEP using a molar ratio of HNO_3/(TEOS+TEP)=0.05. After mixing all reagents, the sol was cast, tightly sealed and aged at room temperature, followed by 3 day at 60 °C. Then the obtained gel was dried at 120 °C, ball milled and sieved to produce powders ranging from 38 to 74 μm. The glass powder calcined at 700 °C were mixed with 6 wt% polyvinyl alcohol water solution binders and cold-pressed using a laboratory uniaxial hydraulic press into 10 mm × 2 mm disks at pressure of 200 MPa. Finally, the green disks were sintered at 1200 °C for 2 h with a heating rate of 5 °C/min.

2.2. Characterization

Differential thermal analysis (DTA) was carried out in a SDT Q600 simultaneous thermal analyzer. Non-isothermal experiments were performed under an air atmosphere with a heating rate of 5, 10 and 20 °C/min. The activation energy for crystallization (E_a) of both phases was calculated from the relationship between the heating rate (β) and the temperature maximum (T_p) in the exothermic peak of the thermal curves using Kissinger equation [14]:

$$\ln \frac{T_P^2}{\beta} = \frac{E_a}{RT_P} + \text{const} \quad (1)$$

where R is the universal gas constant (8.314 J mol^{-1}).

From the value of the activation energy, the Avrami constant (n) describing the dimensionality of crystal growth can be calculated by the Augis–Bennett equation [15]:

$$n = \frac{2.5}{\Delta\tau_{FWHM}} \times \frac{RT_P^2}{E_a} \quad (2)$$

where $\Delta\tau_{FWHM}$ is the full width of the exothermic peak at the half maximum intensity.

X-ray diffraction (XRD) pattern was obtained in a Bruker D8 Advance X-ray diffractometer using CuKα radiation (λ=1.5406 nm) produced at 40 kV and 40 mA. Data were collected from 10° to 60° (2θ) with a step size of 0.02°. Fourier transform infrared spectroscopy (FTIR) analysis was made on a Bruker Optics VERTEX-70 FT-IR spectrometer using the KBr pellets with a transmission mode. The resolution used was 4 cm^{-1} and the number of scans was 32. Scanning electron microscopy (SEM) in a JEOL-JSM 6380LA system working at 20 kV was used to characterize the samples microstructure. Specimens were prepared with standard metallographic techniques by chemical etching in an HF solution (5%) for 90 s. And before tests etched samples were coated with a thin film of gold.

2.3. Degradation and in vitro assays

For degradation studies, the samples were soaked in Tris–HCl solution (pH 7.4), at 37 °C, using triplicate samples. After the set soaking time, samples were rinsed with acetone and dried in air at room temperature. Finally, the weight of each sample was accurately measured using a type of FA2104 electronic balance with an accuracy of 0.1 mg, and the samples weight loss was expressed as percentage of the initial weight.

In vitro assays were evaluated in simulated body fluid (SBF), proposed by Kokubo et al. [16], at 37 °C in sterile polyethylene bottles. The SBF solution has a composition and concentration similar to those inorganic parts of human plasma (as shown in Table 2), and it was continuously replaced every 2 days. Finally, the samples were extensively rinsed with deionized water and acetone and were dried in air at room temperature before being analyzed.

Table 1
Samples chemical composition (mol%).

Sample	CaO	MgO	SiO_2	P_2O_5
S1	38	0	58	4
S2	33	5	58	4
S3	28	10	58	4
S4	18	20	58	4

Table 2
Ion concentration of simulated body fluid and human blood plasma (mM) [16].

	Na^+	K^+	Mg^{2+}	Ca^{2+}	Cl^-	HCO_3^-	HPO_4^{2-}	SO_4^{2-}
SBF	142.0	5.0	1.5	2.5	147.8	4.2	1.0	0.5
Human plasma	142.0	5.0	1.5	2.5	103.0	27.0	1.0	0.5

3. Results and discussion

3.1. Thermal analysis

DTA curves of the dry gel powders containing various amounts of MgO are shown in Fig. 1. It is investigated that the distinct exothermic peak, representing the crystallization peak temperature (T_p), shifts to higher temperature with the addition of MgO in the samples composition. This behavior can be explained by the Dietzel's ionic field strength I ($I=Z/r^2$, where Z and r are the cation charge and radius, respectively). McMillan found that I of network modifier cations was less than 5 $Å^{-2}$ [17], the I of Ca^{2+} and Mg^{2+} is 2.04 $Å^{-2}$ and 4.73 $Å^{-2}$, respectively. Thus, CaO and MgO should insert into glass structure as network modifier and reduce the glass melting point and viscosity [18]. In addition, it is suggested that the glass modifying character of Ca^{2+} is larger than Mg^{2+}.

Crystallization activation energies (E_a) for samples were evaluated from the nonisothermal measurements using Eq. (1). The plots of $\ln(T_p^2/\beta)$ versus $1/T_p$ are shown in Fig. 2, and the related results are inserted into Table 3. It is indicated that the gradual addition of MgO into the base glass, up to 10 mol%, makes the activation energy for crystallization reduce, but more addition induces it increase again. Using activation energy value, the Avrami constant (n) corresponding to the crystallization mechanism was then determined. The value of n close to one means that one-dimension growth (surface crystallization)

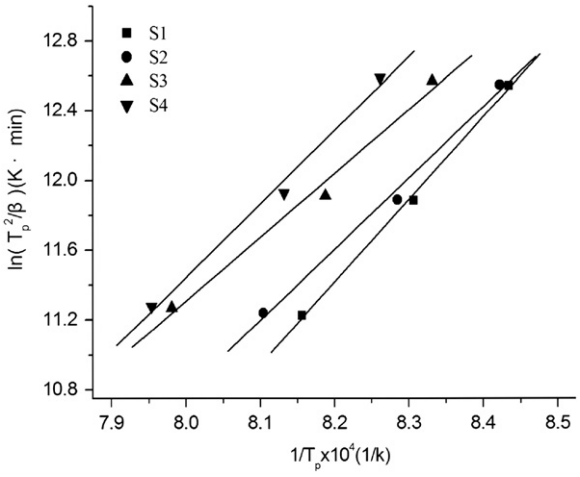

Fig. 2. Plots of $\ln(T_p^2/\beta)$ versus $1/T_p$ for all samples.

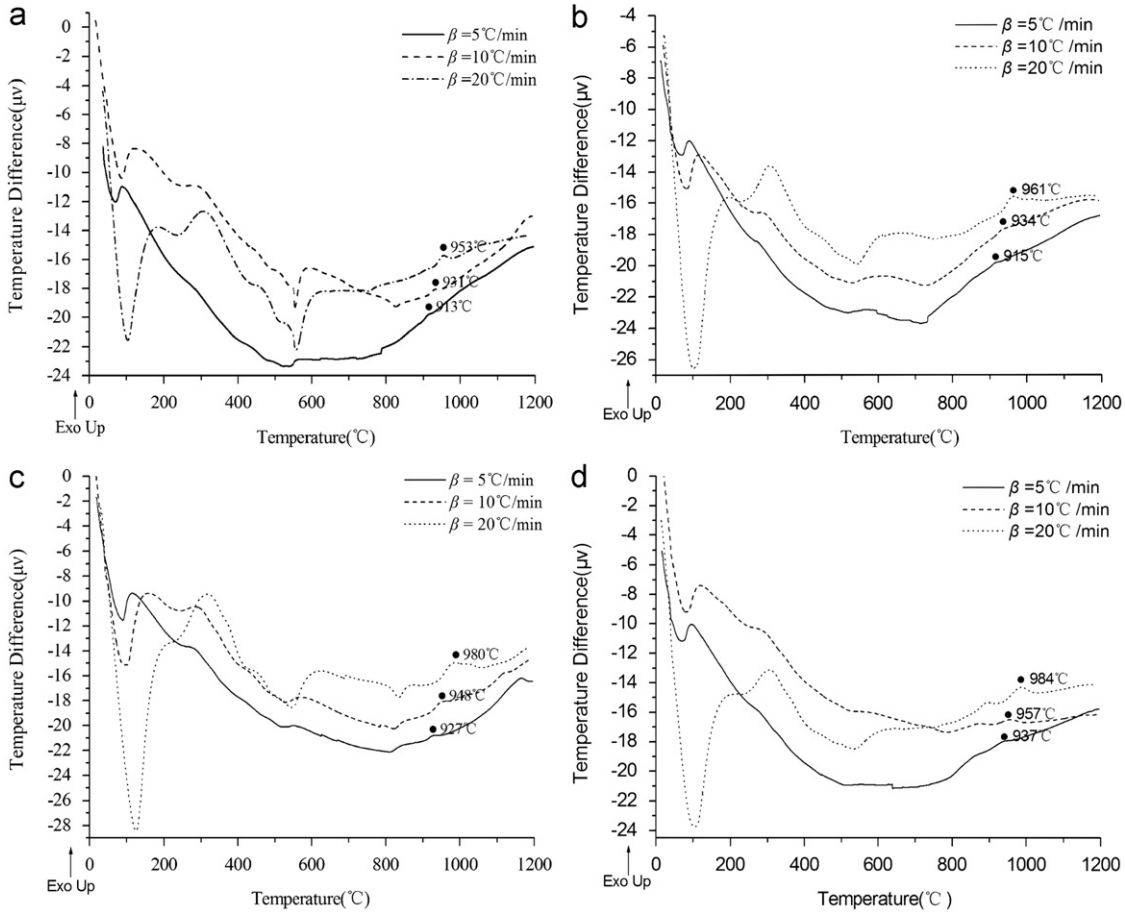

Fig. 1. DTA curves of (a) S1, (b) S2, (c) S3 and (d) S4 dry gel at various heating rates.

dominates overall crystallization, the value of two indicates two-dimension crystallization, the value of three implies a significant contribution of three-dimension growth (bulk crystallization), and the value of four indicates homogeneous crystallization [19–22]. As shown in Table 3, the value of n gradually decreases and the samples crystallization mechanism changes from bulk or homogeneous crystallization to surface crystallization with the MgO addition.

Table 3
Activation energy (E_a) and Avrami constant (n) for crystal growth.

Sample	β (°C/min)	E_a (kJ/mol)	n
	5		5.5
S1	10	398	3.9
	20		3.0
	5		4.8
S2	10	354	3.3
	20		2.5
	5		4.1
S3	10	326	2.9
	20		2.3
	5		2.2
S4	10	349	2.1
	20		1.9

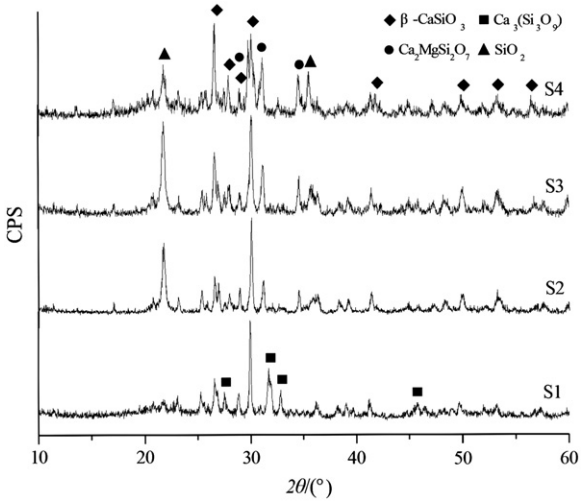

Fig. 3. XRD patterns of glass ceramics heat-treated at 1200 °C.

3.2. Structural and Morphological characterization

XRD patterns of the glass ceramics heat-treated at 1200 °C are presented on Fig. 3. The main phases of wollastonite-2 M β-$CaSiO_3$ (JCPDS 42–0547) and pseudowollastonite $Ca_3(Si_3O_9)$ (JCPDS 74–0874) were observed in the MgO-free glass ceramics S1. For samples S2, S3 and S4 containing various MgO, it is observed that the composition of Mg can react with Ca, Si and O forming a new crystal phase of akermanite $Ca_2MgSi_2O_7$ (JCPDS 35–0592), and with more MgO addition, the content of $Ca_2MgSi_2O_7$ increased at the expense of β-$CaSiO_3$. Moreover, the addition of MgO induced the crystallization of cristomalite SiO_2 (JCPDS 27–0605).

As we known, wollastonite-2M and pseudowollastonite is respectively low and high temperature form of wollastonite. The polymorphic transition of wollastonite-2M to pseudowollastonite in $CaSiO_3$ with high purity takes place at 1130 ± 5 °C. And, it is reported that the presence of Mg is solid solution in wollastonite-2M ($Ca_{1-x}Mg_xSiO_3$; $0 \leqq x \leqq 0.17$) shifts the transition temperature to 1370 ± 20 °C [23]. Thus, when taking into account the solid solution of magnesium in wollastonite-2M, it is reasonable to understand the disappearance of pseudowollastonite in MgO-containing glass ceramics. Moreover, it is known that Ca^{2+} and Mg^{2+}, whose ion radius is respectively 0.99 Å and 0.65 Å, possess the similar coordinator polyhedron in crystal spatial structure. When entering into wollastonite structure, magnesium ion will replace the position of calcium ion and form a substitutional solid solution. In order to study the structure impact of magnesium doping, calculation of the lattice parameters for wollastonite-2M in glass ceramics were carried out by using XRD peaks and the results are listed in Table 4. The values of a-axis and c-axis declined and the elongation of c-axis was observed, however, the changes were less than 5%, suggesting that the doping of magnesium caused no obvious change in wollastonite-2M structure.

Table 4
Lattice parameters for wollastonite-2M in glass ceramics containing various MgO.

	Lattice parameters					
	a (Å)	b (Å)	c (Å)	α (°)	β (°)	γ (°)
Standard JCPDS 42–0547	10.104	11.054	7.305	99.53	100.56	83.44
Calculated from XRD pattern for wollastonite-2M in S1	10.135	11.029	7.329	99.55	100.77	83.62
Calculated from XRD pattern for wollastonite-2M in S2	10.105	11.041	7.312	99.53	100.54	83.33
Calculated from XRD pattern for wollastonite-2M in S3	10.090	11.032	7.293	99.31	100.73	83.51
Calculated from XRD pattern for wollastonite-2M in S4	10.096	11.075	7.324	99.34	100.64	83.53

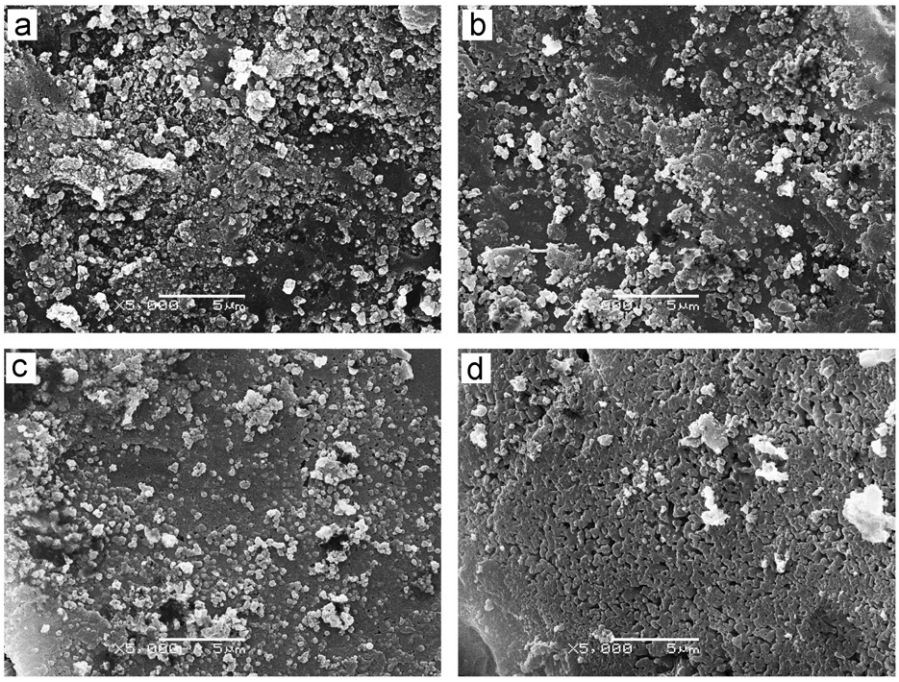

Fig. 4. SEM photographs of (a) S1, (b) S2, (c) S3 and (d) S4 heat-treated at 1200 °C for 2 h.

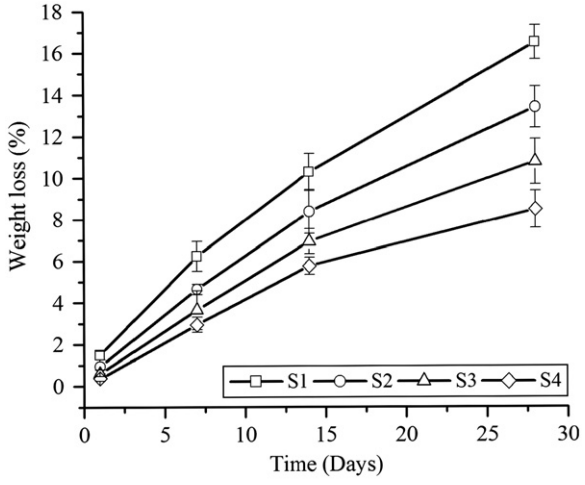

Fig. 5. Weight loss of glass ceramics during soaking in Tris–HCl solution.

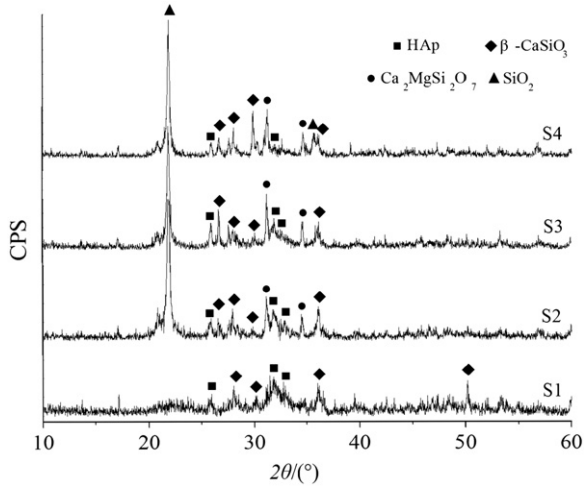

Fig. 6. XRD patterns of glass ceramics after soaking in SBF for 14 days.

Fig. 4 illustrates SEM micrographs of the glass ceramics. As shown in Fig. 4(a), (b) and (c), glass ceramics S1, S2 and S3 presented tiny spherical crystallites and the grain sizes were about 0.5 μm, indicating the homogeneous crystallization behavior. With even more MgO addition, as in Fig. 4(d), the dendritic crystals instead of homogeneous spherical crystallites were observed. Those results are agreement with the above analysis of the samples crystallization kinetics. Namely, the glass samples crystallization mechanism gradually changes from homogeneous crystallization to surface crystallization with the MgO addition.

3.3. Degradation and in vitro assays

The weight losses of glass ceramics after soaking in Tris–Hcl solution are given in Fig. 5. As can be seen, the weight loss of each sample increased with the soaking time. After soaking for 28 days, the MgO-free glass ceramics S1 showed the highest weight loss (17%) and the glass ceramics S4 with the most MgO content presented the lowest weight loss (8%). According to the above analysis, it seems that the glass ceramics degradability correlates to its MgO content. In the XRD patterns (Fig. 3), for MgO-containing glass ceramics (S2, S3 and S4), phases of

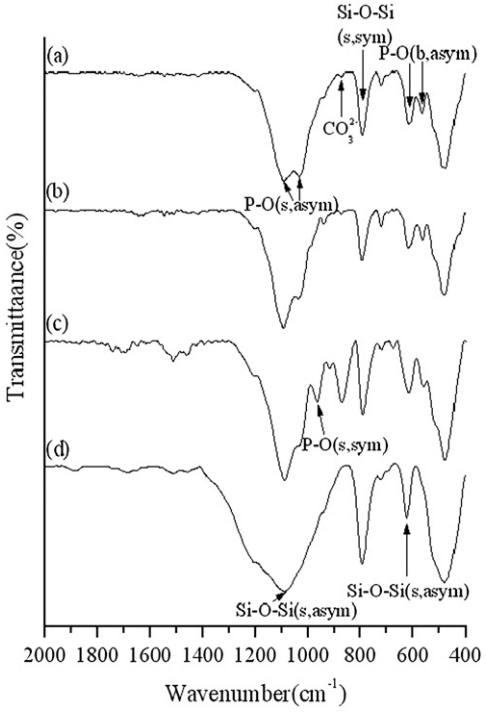

Fig. 7. FTIR spectrum of glass ceramics (a) S1, (b) S2, (c) S3 and (d) S4 after soaking in SBF for 14 days.

$Ca_2MgSi_2O_7$ and SiO_2 were also investigated besides β-$CaSiO_3$, and the content of $Ca_2MgSi_2O_7$ increased with the decline of the β-$CaSiO_3$. It is known that the phase of SiO_2 is a bioinert material, $Ca_2MgSi_2O_7$ has been proved to be bioactive and its degradation rate is significantly lower than that of β-$CaSiO_3$ [24]. Therefore, it is comprehensible that the role of MgO addition in altering the degradability of synthesized glass ceramics is mainly achieved by the formation of $Ca_2MgSi_2O_7$ and SiO_2 phases.

β-$CaSiO_3$ and $Ca_3(Si_3O_9)$ are the most common calcium silicate biomaterials proposed for bone tissue regeneration, because of their good biocompatibility and bioactivity [25,26]. However, major drawback of $CaSiO_3$ bioceramics is their relatively fast dissolution rate that could comprise theirs mechanical strength. In addition, the pH of the surrounding medium significantly increases which could affect the osseointegration of the substitute material within the natural bone [27,28]. In this work, β-$CaSiO_3$–$Ca_2MgSi_2O_7$-based glass ceramics were obtained and the degradation rate adjustment was achieved by the MgO contents modulation. On the other hand, especially from the perspective of bone tissue repair applications, bioceramics with various degradation rates are needed for different planting patients and sites, β-$CaSiO_3$–$Ca_2MgSi_2O_7$-based glass ceramics can be one potential candidate.

XRD patterns of glass ceramics after 14 days of soaking in SBF are given in Fig. 6. Besides the original phase of β-$CaSiO_3$, the diffraction peaks at 25.7, 31.9 and 32.8° 2θ corresponding to (002), (211) and (300) reflections of an apatite phase were detected on the X-ray diffraction pattern of the glass ceramic S1. The results also justify that $Ca_3(Si_3O_9)$ has higher dissolution rate in SBF solution than β-$CaSiO_3$. For other samples, the presence of an apatite phase was also observed, however, the intensity of apatite peaks declined with the increase in MgO content. It seems that the samples apatite-formation ability has some relationship with its degradability, a lower value of degradability suggests a lower formation rate of apatite.

FTIR spectra of glass ceramics after soaking in the SBF solution were also recorded. After soaking, glass ceramics S1, S2 and S3 displayed the obvious doublet bands at 601 and 568 cm^{-1} (Fig. 7(a), (b) and (c)), which are assigned to crystalline calcium phosphate [29,30]. However, these above bands are not clearly in glass ceramics S4 (Fig. 7(d)). In addition, the vibration bands corresponding to the carbonate groups around at 1490, 1423 and 874 cm^{-1} were also found in the spectra of all samples after soaking. The appearance of phosphate and carbonate absorption bands in the samples spectra after soaking in SBF not only confirms the formation of an apatite layer but also reveals that the newly formed material is a carbonated hydroxyapatite. The samples surface morphologies after soaking in SBF for 14 days were also detected, as shown in Fig. 8. The MgO-free glass ceramics S1 was fully covered by an apatite layer constituted by numerous aggregates of spherical and lathlike crystals (Fig. 8(a, b). Such similar morphologies were also observed on glass ceramics S2 and S3 (Fig. 8(c, d) and (e, f)). However, unlike the above-mentioned morphologies, after soaking for 14 days, the formation of apatite was slight on the surface of glass ceramics S4 with most MgO content (Fig. 8(g and h)).

4. Conclusions

β-$CaSiO_3$–$Ca_2MgSi_2O_7$ glass ceramics were obtained by sintering CaO–MgO–SiO_2–P_2O_5 glass system with MgO addition. As the MgO content increased, the glass crystallization temperature increased and the crystallization of the glass ceramics changed from bulk crystallization to surface crystallization. The obtained degradation and in vitro assay results indicated that the addition of MgO slowed down the rate of samples dissolution and retarded the formation of apatite layer. Those influences are mainly due to the formation of $Ca_2MgSi_2O_7$ and SiO_2, moreover, it is indicated that the controlled rates of dissolution and apatite formation of these bioactive glass ceramics were possible to design.

Acknowledgments

This work was financially supported by the Department of Science and Technology of Shandong Province (Grant no. 2006GG3203006, 2009GG10003032), PR China.

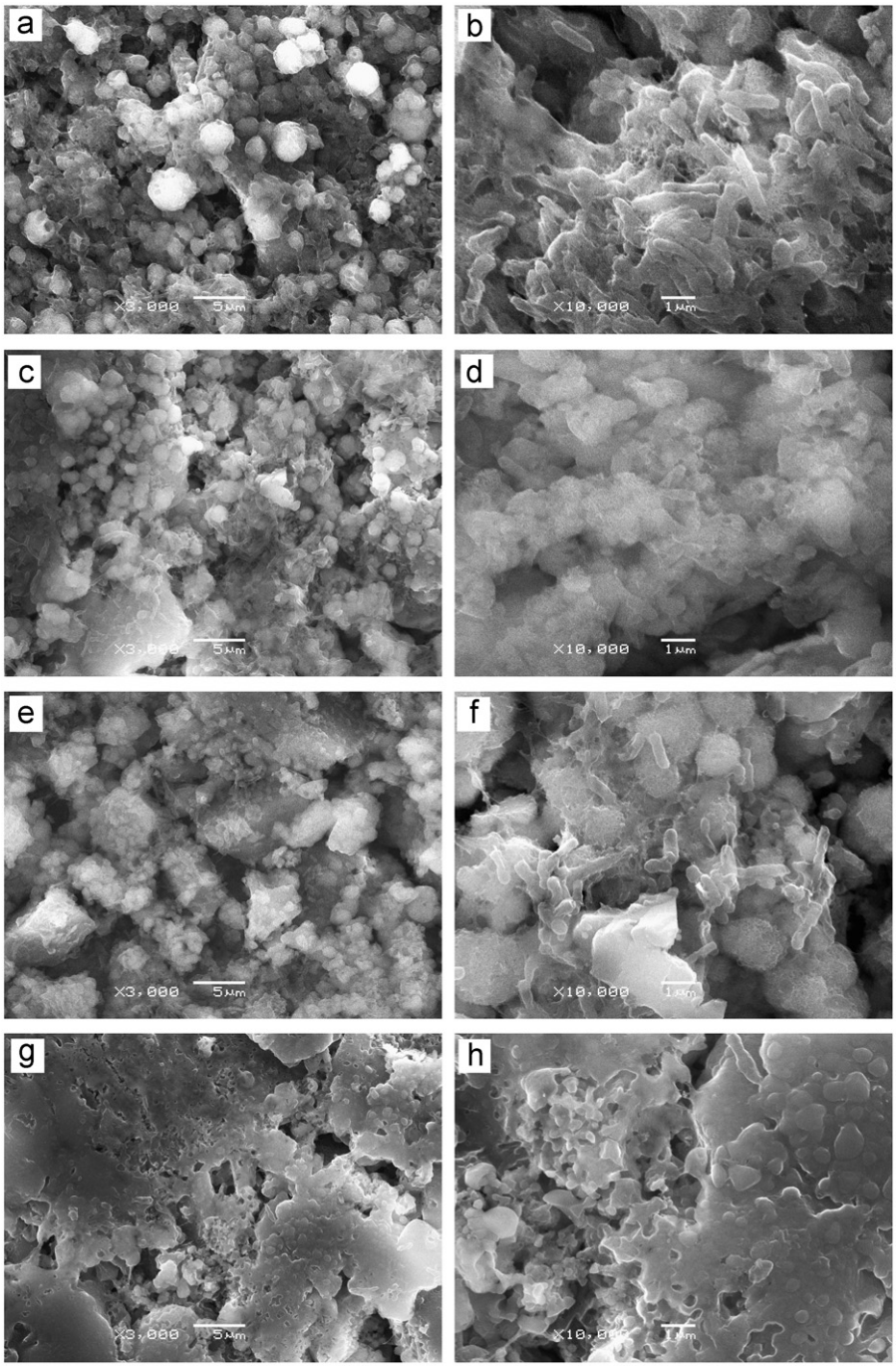

Fig. 8. SEM photographs of glass ceramics S1 (a and b), S2 (c and d), S3 (e and f) and S4 (g and h) after soaking in SBF for 14 days.

References

[1] L.L. Hench, Bioactive glasses and glass-ceramics, Materials Science Forum 293 (1999) 37–64.

[2] T. Kokubo, H.M. Kim, M. Kawashita, Novel bioactive materials with different mechanical properties, Biomaterials 24 (2003) 2161–2175.

[3] C. Vitale-Brovarone, E. Vernè, M. Bosetti, P. Appendino, M. Cannas, Microstructural and in vitro characterization of SiO_2–Na_2O–CaO–MgO glass-ceramic bioactive scaffolds for bone substitutes, Journal of Materials Science: Materials in Medicine 16 (2005) 909–917.

[4] W. Xia, J. Chang, Preparation, in vitro bioactivity and drug release property of well-ordered mesoporous 58S bioactive glass, Journal of Non-Crystalline Solids 354 (2008) 1338–1341.

[5] R.L. Du, J. Chang, S.Y. Ni, W.Y. Zhai, J.Y. Wang, Characterization and in vitro bioactivity of zinc-containing bioactive glass and glass-ceramics, Journal of biomaterials applications 20 (2006) 341–360.

[6] T. Sun, H.N. Xiao, Y. Cheng, H.B. Liu, Effects of MO (M = Ba, Mg, Ca) on the crystallization of B_2O_3–Al_2O_3–SiO_2 glass-ceramics, Ceramics International 35 (2009) 1051–1055.

[7] H.S. Ryu, J.K. Lee, J.H. Seo, H. Kim, K.S. Hong, D.J. Kim, J.H. Lee, B.S. Chang, C.K. Lee, S.S. Chung, Novel bioactive and biodegradable glass ceramics with high mechanical strength in the

$CaO–SiO_2–B_2O_3$ system, Journal of Biomedical Materials Research Part A 68 (2004) 79–89.

[8] J. Althoff, P. Quint, E.R. Krefting, H.J. Höhling, Morphological studies on the epiphyseal growth plate combined with biochemical and X-ray microprobe analyses, Histochemistry and Cell Biology 74 (1982) 541–552.

[9] J.M. Oliveira, R.N. Correia, M.H. Fernandez, J. Rocha, Influence of the CaO/MgO ratio on the structure of phase-separated glasses: a solid state ^{29}Si and ^{31}P MAS NMR study, Journal of Non-Crystalline Solids 265 (2000) 221–229.

[10] C.T. Wu, J. Chang, J.Y. Wang, S.Y. Ni, W.Y. Zhai, Preparation and characteristics of a calcium magnesium silicate (bredigite) bioactive ceramics, Biomaterials 26 (2005) 2925–2931.

[11] F. Barrere, C.A van Blitterswijk, K de.Groot, P. Layrolle, Nucleation of biomimetic Ca–P coationgs on Ti6Al4V from a SBF × 5 solution: influence of magnesium, Biomaterials 23 (2002) 2211–2220.

[12] J. Roman, A.J. Salinas, M. Vallet-Regi, J.M. Oliveira, R.N. Correia, M.H. Fernandes, Role of acid attack in the in vitro bioactivity of a glass-ceramic of the $3CaO \cdot P_2O_5–CaO \cdot SiO_2–CaO \cdot MgO \cdot 2SiO_2$ system, Biomaterials 22 (2001) 2013–2019.

[13] J. Pérez-Pariente, F. Balas, J. Román, A.J. Salinas, M. Vallet-Regí, Influence of composition and surface characteristics on the in vitro bioactivity of $SiO_2–CaO–P_2O_5–MgO$ sol-gel glasses, Journal of Biomedical Materials Research 47 (1999) 170–175.

[14] H.E. Kissinger, Variation of peak temperature with heating rate in differential thermal analysis, Journal of research of the National Bureau of Standards 57 (1956) 17–21.

[15] J.A. Augis, J.E. Bennett, Calculation of the Avrami parameters for heterogeneous solid-state reactions using a modification of the Kissinger method, Journal of Thermal Analysis 13 (1978) 283–292.

[16] T. Kokubo, H. Kushitani, S. Sakka, T. Kitsugi, Yamamuro, Solutions able to reproduce in vivo surface-structure changes in bioactive glassceramic A-W^3, Journal of Biomedical Materials Research 24 (1990) 721–734.

[17] P.W. McMillan, Glass-ceramics, Academic press, London, New York, 1964.

[18] A.M. Hu, M. Li, D.L. Mao, Growth behavior, morphology and properties of lithium aluminosilicate glass ceramics with different amount of CaO, MgO and TiO_2 additive, Ceramics International 34 (2008) 1393–1397.

[19] D.C. Clupper, L.L. Hench, Crystallization kinetics of tape cast bioactive glass 45S5, Journal of Non-Crystalline Solids 318 (2003) 43–48.

[20] J. Ma Rincon, M. Romero, J. Marco, V. Caballer, Some aspect of crystallization microstructure on new glass-ceramic glazes, Materials Research Bulletin 33 (1998) 1159–1164.

[21] A.W.A EI-Shennawi, E.M.A Hamzawy, G.A. Khater, A.A Omar, Crystallization of some aluminosilicate glasses, Ceramics International 27 (2001) 725–730.

[22] M. Romero, J. Ma Rincón, A. Acosta, Effect of iron oxide content on the crystallisation of a diopside glass-ceramic glaze, Journal of the European Ceramic Society 22 (2002) 883–890.

[23] M.A. Sainz, P. Pena, S. Serena, A. Caballero, Influence of design on bioactivity of novel $CaSiO_3$-$CaMg(SiO_3)_2$ bioceramics: In vitro simulated body fluid test and thermodynamic simulation, Acta Biomaterialia 6 (2010) 2797–2807.

[24] C.T. Wu, J. Chang, Degradation, bioactivity and cytocompatibility of diopside, akermanite and bredigite ceramics, Journal of Biomedical Materials Research Part B 83 (2007) 153–160.

[25] S. Nita, A. Michel, Cyclic silicate active site and stereochemical match for apatite nucleation on pseudowollastonite bioceramic-bone, Biomaterials 26 (2005) 5763–5770.

[26] K.L. Lin, W.Y. Zhi, S.Y. Ni, J. Chang, Y. Zeng, W.J. Qin, Study og the mechanical property and invitro biocompatibility of $CaSiO_3$ ceramics, Ceramics International 31 (2005) 323–326.

[27] Y. Iimori, Y. Kameshima, K. Okada, S. Hayashi, Comparative study of apatite formation on $CaSiO_3$ ceramics in simulated body fluids with different carbonate concentrations, Journal of Materials Science: Materials in Medicine 16 (2005) 73–79.

[28] A. El-Ghannam, P. Ducheyne, I.M. Shapiro, Porous bioactive glass and hydroxyapatite ceramic affect bone cell function in vitro along different time lines, Journal of Biomedical Materials Research 36 (1997) 167–180.

[29] C. Ohtsuki, T. Kokubo, T. Yamamuro, Mechanism of apatite formation on $CaO–SiO_2–P_2O_5$ glasses in a simulated body fluid, Journal of Non-Crystalline Solids 143 (1992) 84–92.

[30] P. Li, C. Ohtsuki, T. Kokubo, K. Nakanishi, N. Soga, T. Nakamura, T. Yamamuro, Process of formation of bone-like apatite layer on silica gel, Journal of Materials Science: Materials in Medicine 4 (1993) 127–131.